RSC Advances

PAPER

View Article Online
View Journal | View Issue

Cite this: *RSC Adv.*, 2026, **16**, 13369

Synthesis and biological evaluation of *N*/*O*-propargylated diarylpyrimidines as dual inhibitors of acetylcholinesterase and monoamine oxidase

Naveen Kumar,[a] Kailash Jangid,[ab] Vijay Kumar,[a] Ashish Ranjan Dwivedi,[bd] Vinay Kumar,[a] Bharti Devi,[a] Tania Arora,[c] Jyoti Parkash[c] and Vinod Kumar *[a]

Alzheimer's disease is a complex neurological disorder and is becoming a global health concern as the population ages. Considering the complex aetiology of the disease and ineptness of single-targeted drugs, the development of multi-targeted drugs emerges as the most effective strategy for the treatment of the disease. Cholinesterases and monoamine oxidases are amongst the most widely explored targets in Alzheimer's disease, and their dual inhibition offers a promising approach for achieving multipotent therapeutic effects. Herein, we designed and synthesized a series of *N*/*O*-propargylated diaryl pyrimidines and evaluated their inhibitory activity against acetylcholinesterase (AChE) and monoamine oxidase (MAO) enzymes. Most of the compounds were found to be active against AChE, MAO-A and MAO-B. Amongst the synthesised derivatives of the series, compounds, compounds **NV-1** and **NV-9** exhibited a balanced multipotent activity profile against both the targets *i.e.* acetylcholinesterase and monoamine oxidase. Compounds **NV-1** and **NV-9** displayed IC_{50} values of 1.30 μM and 0.88 μM against AChE, 0.232 μM and 9.31 μM against MAO-A and 0.949 μM and 9.23 μM against MAO-B, respectively. In the reversibility inhibition studies, both the compounds were found to be reversible in nature. In kinetic inhibition studies, both **NV-1** and **NV-9** showed non-competitive inhibition for AChE. Additionally, **NV-1** and **NV-9** were found to be moderately neuroprotective in nature and exhibit no cytotoxicity at lower compound concentrations. In the partition coefficient studies (octanol/water), the compound **NV-9** was found to be lipophilic in nature. Molecular docking studies illustrate their stability within the active cavity of both enzymes. Simulation studies confirmed the thermodynamic stability of these compounds within the cavity for up to 100 ns. Thus, the *N*/*O*-propargylated diarylpyrimidines have the potential to be developed as multipotent drugs for the treatment of Alzheimer's disease.

Received 10th November 2025
Accepted 16th February 2026

DOI: 10.1039/d5ra08679e

rsc.li/rsc-advances

Introduction

Alzheimer's disease (AD) is a severe neurological condition,[1] and more than 50 million people are affected worldwide. It is the most common cause of dementia that causes memory loss and cognitive impairment[2] by the degeneration of the neuronal cells, causes continuous declining of thinking, communication, and social skills, and affects the normal functioning of daily life.[3] The available treatments give only symptomatic relief, and there is no drug available for the complete eradication of the disease.[4] The aetiology of Alzheimer's disease is complex in nature,[5] and many pathological targets are involved in the initiation and progression of the disease, including increased acetylcholinesterase (AChE) inhibitor concentration, over-activation of monoamine oxidase (MAO) enzyme, excess formation of amyloid plaques and tangled clumps of tau protein, disruption of glutaminergic and adrenergic systems, metal ion dyshomeostasis and increased reactive oxygen species (ROS) levels.[6,7] Because of the complex aetiology of Alzheimer's disease and the involvement of many pathological targets, the development of multi-target-directed ligands (MTDLs) for the simultaneous inhibition of two or more targets is proposed as an effective treatment strategy.[8]

Pyrimidine scaffold is an important part of DNA and RNA involved in almost all the biological systems.[9] Many pyrimidine-based derivatives have been designed, synthesized, and evaluated as anti-Alzheimer agents.[10] Aryl substitution at the different positions of the pyrimidine scaffold have shown different biological activities.[11,12] S. Ahmad *et al.* designed and synthesized dihydropyrimidine derivatives as dual binding (AChE and BuChE) inhibitors with good binding affinity to the

[a]*Laboratory of Organic and Medicinal Chemistry, Department of Chemistry, Central University of Punjab, Bathinda, Punjab, 151401, India. E-mail: vpathania18@gmail.com; vinod.kumar@cup.edu.in; Tel: +911642864269*

[b]*Department of Pharmaceutical Sciences and Natural Products, Central University of Punjab, Bathinda, Punjab, 151401, India*

[c]*Department of Zoology, Central University of Punjab, Bathinda, Punjab, 151401, India*

[d]*Gitam School of Pharmacy, Hyderabad, Telangana, 502329, India*

key amino acid residues of the catalytic active site (CAS) and peripheral anionic site (PAS) of AChE.[13] Manzoor and group reported phenyl-sulfonyl substituted pyrimidine carboxylate derivatives as potential multi-target leads for the inhibition of AChE and AChE-induced amyloid-β aggregation. Almost all the compounds of the series showed selective AChE inhibition over BuChE in higher nanomolar range.[14] Pyrimidine-triazolopyrimidine and pyrimidine-pyridine-based hybrid scaffolds were synthesized and screened against cholinesterase enzymes, showing IC_{50} values in the nanomolar range and interactions with both the CAS and PAS of AChE.[15] Blood–brain barrier (BBB) permeability is one of the major challenges in AD drug discovery. A series of novel propargylamine-modified aminoalkyl imidazole-substituted pyrimidinylthiourea derivatives were screened as multifunctional agents for potential drug-likeness, low cytotoxicity, and enhanced BBB permeability. The lead compound from this series was reported to ameliorate scopolamine-induced cognitive impairment in a mouse model of Alzheimer's disease.[16] Nadeem *et al.* reported variation in several functionalities and linker lengths in indole-containing 2-arylidine derivatives of thiazolopyrimidine that showed enhanced cholinesterase and monoamine oxidase inhibition activities along with improved BBB permeability and no cytotoxicity to the neuronal cells.[17] Javed *et al.* synthesised and biologically evaluated a series of pyrimidine/pyrrolidine-sertraline hybrids and improved short and long-term memory, and enhanced learning behavior in AD mouse model was observed.[18] Recently, substituted pyrimidine scaffolds were synthesized and studied as potent anti-AD agents using *in vivo* mouse model by Swati and group. The lead molecule showed promising activities comparable to that of the standard.[19]

For the past few years, our laboratory has been working on the design, synthesis, and screening of small organic molecules as multi-target-directed ligands for the treatment of AD. A number of pyrimidine derivatives were synthesized, and a structure–activity relationship profile was developed for the identification of active leads with a balanced multipotent profile against different targets of AD. The propargyl group has been identified as an important pharmacophore[20,21,22] for its interaction with monoamine oxidases, and we are further exploring this moiety in the pyrimidine scaffold. We synthesized diphenyl-substituted pyrimidine derivatives as dual inhibitors of AChE and MAO enzymes. With variation in the substitution pattern, these compounds showed varying activity profiles and potent leads were identified, showing a balanced activity profile against both the enzymes. The identified leads exhibited good neuroprotective potential against SH-SY5Y cells in the 6-OHDA and H_2O_2-induced neurotoxicity.[22,23] Additionally, the lead molecule were evaluated *in vivo* using scopolamine-induced neurotoxicity in mice model of Alzheimer's disease.[24] Recently, a series of phenylstyrylpyrimidine derivatives was synthesized and evaluated as anti-AD agents, exhibiting multipotent profile against AChE, MAO, and self-induced amyloid-β aggregation.[20] Computational studies revealed that the propargyl group strongly interacts with the MAO enzyme, probably through the covalent interaction between its terminal alkyne and the FAD co-factor.[25]

Taking leads from the previous research work done in our laboratory, the computational studies revealed that the pyrimidine moiety usually orients towards the FAD co-factor of the MAO enzyme. In our previous studies,[22,23,24] the propargyl moiety was substituted at the diaryl rings attached to the pyrimidine ring, and many times it orients away from the FAD pocket. The propargyl group is a classified MAO pharmacophore, which is well known for developing mechanism-based inhibitors. Propargylation at the pyrimidine core was designed to generate an MAO-reactive warhead with a rigid heteroaromatic scaffold, exhibiting improved active-site positioning, enabling mechanism-based FAD interaction, and enhanced overall binding and activity toward the MAO enzyme. Thus, in the present study, we incorporated the propargyl moiety on the pyrimidine ring and investigated its impact on the inhibition activity of the target enzymes. The attachment of two phenyl rings to the pyrimidine nucleus provided an elongated structure, which can effectively bind to the PAS and CAS of the AChE enzyme. Most of the synthesized compounds showed potent inhibitory activities against AChE and MAO enzymes at lower to sub-micromolar concentrations. The neuroprotection potential and cytotoxicity of the potent compounds were evaluated against SH-SY5Y neuronal cells. In addition, molecular docking and dynamics simulation studies were performed to assess the binding interactions and stability of the ligands and enzyme–ligand complexes.

Results and discussion

Chemistry

All the compounds were synthesized based on the reaction procedures described in Scheme 1. Briefly, substituted acetophenone and benzaldehydes were reacted in the presence of urea and iodine to produce pyrimidinone, which was chlorinated using $POCl_3$ in toluene. Finally, the chlorinated derivative was substituted with propargyl amine/alcohol in DMF to get the final product. The formation of the product was confirmed by ^1H, ^{13}C, and HMRS data.

Biological results

hMAO and AChE inhibition studies. The evaluation of MAO and AChE inhibition studies of the synthesized compounds is performed through fluorometric absorption methods using Amplex Red[26] and Ellman's assay[27] kits from Molecular Probes (Invitrogen), Life Technologies. The results of these inhibition assays are reported in the form of IC_{50} (μM) values summarised in Table 1. It has been observed that some of the compounds were found to inhibit both MAO and AChE enzymes in the low micromolar range concentration. The aryl rings attached to the pyrimidine scaffold were alternatively substituted (R_1 and R_2) with different groups, including electron-withdrawing and electron-donating substituents, to develop a structure–activity relationship (SAR) profile. As evident from Table 1, compound **NV-1** was found to be the most potent inhibitor of MAO-A and MAO-B isoforms with IC_{50} values of 0.232 μM and 0.949 μM, respectively. It displayed IC_{50} value of 1.30 μM against the AChE

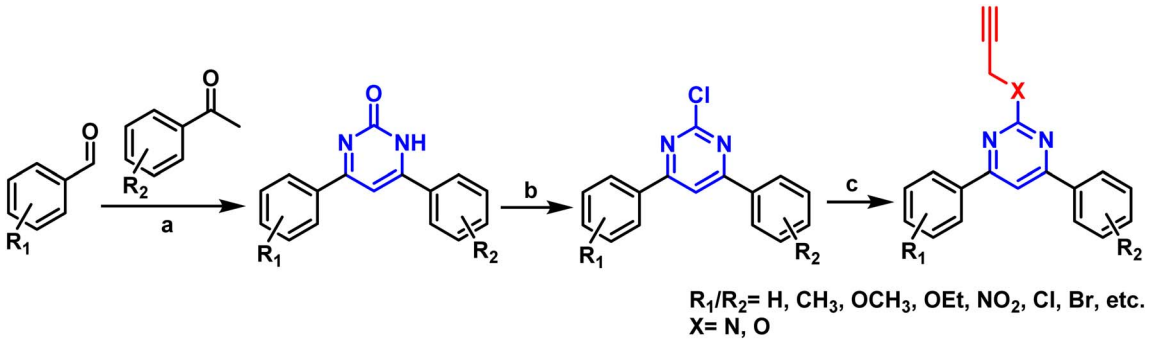

Scheme 1 Synthetic route for diaryl-substituted propargylated pyrimidine derivatives.

enzyme. Similarly, compound **NV-9** was found to be the most potent inhibitor of the AChE enzyme with IC_{50} value of 0.88 μM, and it showed IC_{50} values of 9.31 μM and 9.23 μM against MAO-A and MAO-B isoforms, respectively.

Reversibility inhibition studies. Reversible inhibition studies were conducted to assess whether the compounds were reversible or irreversible inhibitors[28] of AChE and MAO-B enzymes. At IC_{50} concentration, **NV-1** showed 57.43% and

Table 1 Results of the biological inhibition studies of MAO-A, MAO-B and AChE[a]

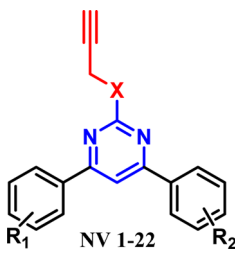

NV 1-22

Entry name	X	R_1	R_2	IC_{50} values (mean ± S.E., μM) hMAO-A	hMAO-B	AChE
NV-1	**N**	**4-CH_3**	**H**	**0.232 ± 0.04**	**0.949** ± 0.001	**1.30 ± 0.01**
NV-2	N	H	3-Br	1.667 ± 0.05	4.429 ± 0.06	8.70 ± 0.02
NV-3	N	4-Cl	4-Br	0.996 ± 0.03	9.728 ± 0.02	3.48 ± 0.012
NV-4	N	4-Cl	H	>10	2.528 ± 0.04	7.00 ± 0.005
NV-5	N	4-Br	4-OMe	>10	12.371 ± 0.1	3.28 ± 0.006
NV-6	N	4-OMe	H	>10	10.459 ± 0.02	4.23 ± 0.006
NV-7	N	4-CH_3	4-OMe	0.805 ± 0.02	13.191 ± 0.1	9.16 ± 0.009
NV-8	N	4-Cl	4-OMe	>10	7.547 ± 0.02	6.30 ± 0.01
NV-9	**N**	**3,4,5-OMe**	**3-NO_2**	**9.31 ± 0.1**	**9.231 ± 0.02**	**0.88 ± 0.013**
NV-10	N	4-CH_3	3-Br	8.80 ± 0.02	13.115 ± 0.17	23.41 ± 0.004
NV-11	O	H	3-Br	9.815 ± 0.02	14.275 ± 0.03	6.56 ± 0.015
NV-12	O	4-OMe	4-OMe	4.90 ± 0.07	>25	26.24 ± 0.015
NV-13	O	4-OMe	4-Cl	>10	5.947 ± 0.02	1.38 ± 0.003
NV-14	O	4-OMe	H	0.808 ± 0.009	>25	6.99 ± 0.007
NV-15	O	H	2,4-Cl	>10	>25	3.26 ± 0.006
NV-16	O	4-OMe	4-Br	>10	8.602 ± 0.048	6.96 ± 0.014
NV-17	O	4-CH_3	3-Br	6.68 ± 0.02	>25	7.75 ± 0.042
NV-18	O	4-CH_3	4-OMe	>10	>25	5.46 ± 0.023
NV-19	O	4-Cl	H	4.38 ± 0.024	>25	8.73 ± 0.038
NV-20	O	3-NO_2	H	7.69 ± 0.08	>25	3.55 ± 0.045
NV-21	O	3-Br	3,4-OMe	15.26 ± 0.31	>25	19.46 ± 0.025
Clorgyline				0.049 ± 0.002	nd	nd
Pargyline				nd	0.072 ± 0.001	nd
Donepezil				nd	nd	0.026 ± 0.003

[a] nd = not determined.

78.92% activity, while **NV-9** showed 65.30% and 55.27% inhibitory activity against AChE and MAO-B, respectively. Inhibition was increased by increasing the concentrations to 10 × IC_{50} and 100 × IC_{50}. The maximum inhibition was achieved at 100 × IC_{50}, where only 7.45% and 7.49% activities were observed for AChE, while 43.92% and 37.39% activities were observed for MAO-B by **NV-1** and **NV-9**, respectively. The activity was recovered by diluting the compounds to a concentration of 0.1 × IC_{50}. A total of 96.56% and 97.45% activity was recovered for AChE and 85.38% and 75.44% activity for the MAO-B enzyme by **NV-1** and **NV-9**, respectively (Fig. 1). This study demonstrates the reversible nature of both the inhibitors against AChE and MAO-B enzymes.

Kinetic studies of VAChE inhibition. Kinetic studies were performed with the lead compounds **NV-1** and **NV-9** against AChE to determine the mechanism of inhibition.[28] From the reciprocal Lineweaver–Burk plots, it was observed that with an increase in the concentration of the compound, reduced V_{max} and unaffected K_m values are obtained, as shown in Fig. 2. The intercept of the double reciprocal Lineweaver–Burk plot is on the *x*-axis, showing that the reaction follows non-competitive inhibition. Therefore, the lead compounds **NV-1** and **NV-9** have an affinity to bind to free enzymes on a site other than the active site (allosteric site) and thus reduce the enzyme's ability to catalyse the reaction regardless of the substrate concentration.

Neuroprotective effects. The most potent compounds (**NV-1** and **NV-9**) were evaluated for their neuroprotection potential using neurotoxin 6-hydroxydopamine (6-OHDA) on human neuroblastoma SH-SY5Y cells. Compound **NV-9** did not show any neuroprotective effects, while **NV-1** displayed moderate neuroprotective potential against the 6-OHDA neurotoxin. As the concentration of the inhibitor increases from 0.1 μM to 10 μM, the percentage cell viability also increases. As depicted in Fig. 3, compound **NV-1** showed a maximum percentage cell viability of 63.97%, while **NV-9** showed a maximum cell viability of 51.57%. Therefore, the compounds exhibited only moderate neuroprotective potential.

Cytotoxicity studies. To assess the cell viability, the lead compounds (**NV-1** and **NV-9**) were evaluated for their cytotoxicity against neuronal cells (SH-SY5Y). The test compounds at 0.1 μM, 1 μM and 10 μM concentrations were incubated for 24 h with SH-SY5Y cells, and the viability of the cells was determined using the MTT assay, as shown in Fig. 4. With the increase in the concentration of the test compounds, the percentage cell viability decreases. The compounds were found to be non-toxic at lower concentrations. Compound **NV-1** showed a minimum cell viability of 51.38% at 10 μM, whereas it showed a maximum cell viability of 61.36% at the lowest (0.1 μM) compound concentration. As more than 50% cell viability was observed even with the highest compound concentration (10 μM), so, the

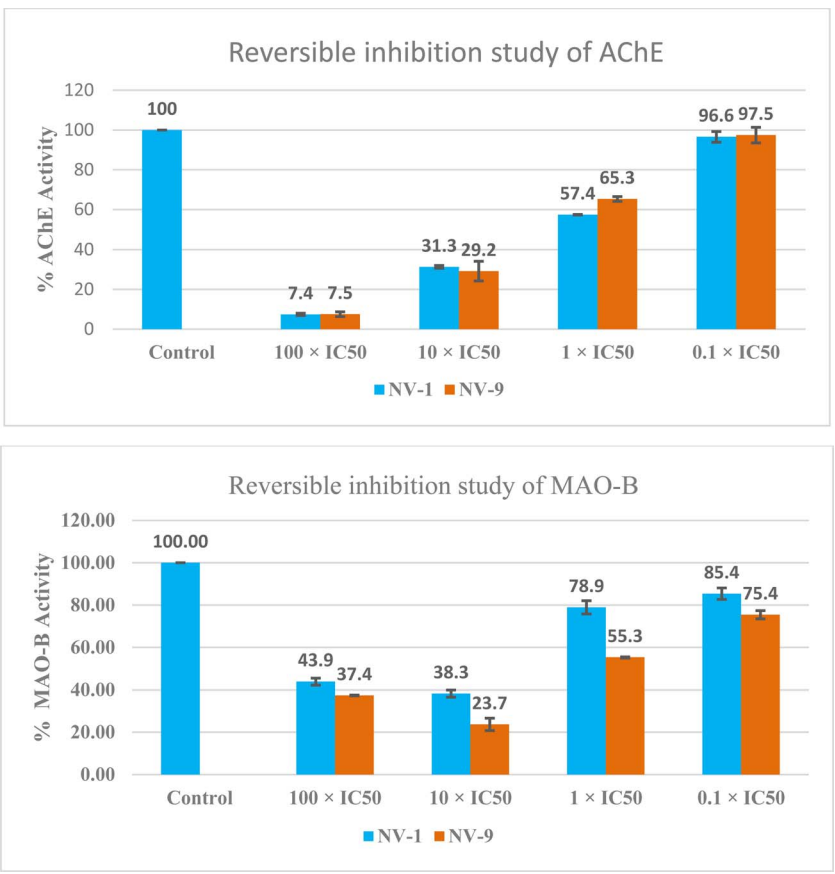

Fig. 1 Reversibility inhibition study of **NV-1** and **NV-9** for AChE and MAO-B enzymes.

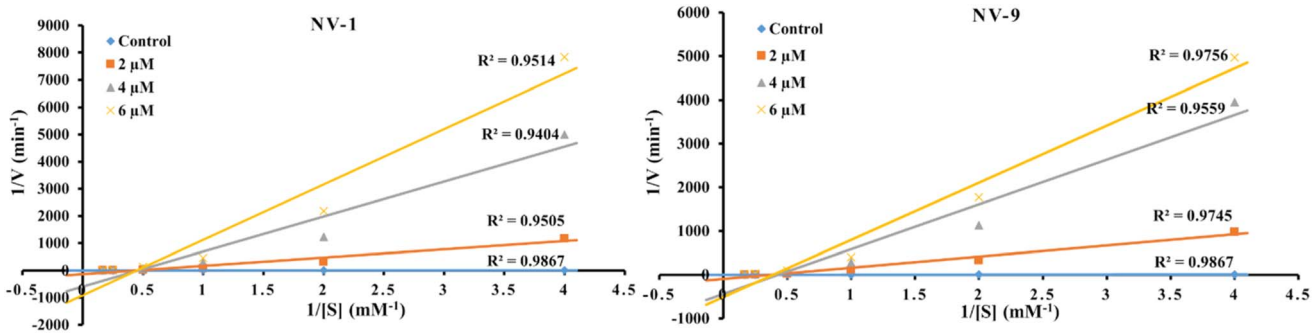

Fig. 2 Kinetic studies on the AChE inhibition mechanism by **NV-1** and **NV-9**. Lineweaver–Burk plots of AChE initial velocities at increasing substrate concentrations (0.25–6 mM) in the presence and absence of the inhibitors.

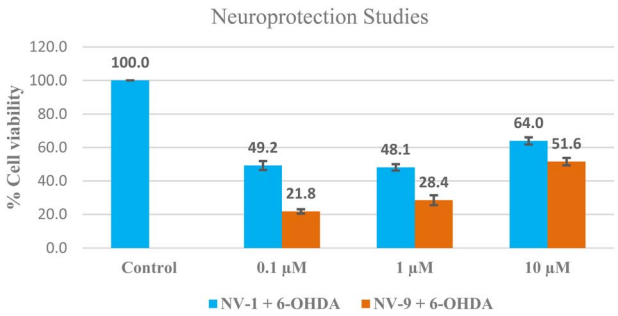

Fig. 3 Neuroprotective studies of **NV-1** and **NV-9** against SH-SY5Y cells.

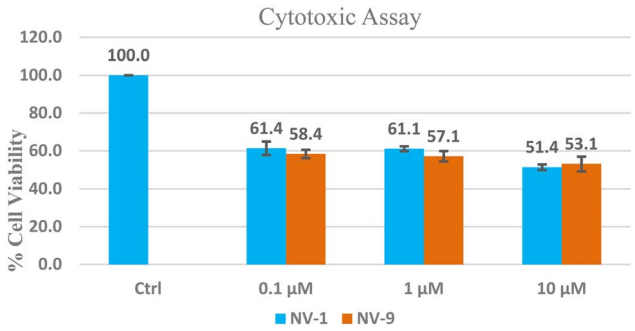

Fig. 4 Cytotoxicity studies of **NV-1** and **NV-9** against SH-SY5Y cells after 24 h of treatment.

lower micromolar IC_{50} values of the synthesized compounds suggest minimal cytotoxic effects on the neuronal cell lines.

Molecular docking. Molecular docking is an important tool for understanding the interactions between target proteins and test molecules. It provides information about the orientation of the test molecules and their interactions with amino acids in the active cavity of the enzyme.[29] All the synthesized compounds of the series were docked against AChE (PDB ID-1EVE co-crystallised with donepezil) to know the binding interactions with the active sites of AChE. The docking studies were performed using Maestro 12.8 (Schrodinger LLC) software. The interactions and alignments of the most active compounds, **NV-1** and **NV-9**, from *in vitro* studies are depicted in Fig. 5. The active site of AChE is divided into two compartments, namely, the catalytic active site (CAS) and peripheral anionic site (PAS). The CAS is mainly composed of Trp84, Tyr130, Phe330, Phe331, and the PAS consists of Tyr70, Asp72, Tyr121, Trp279, and Tyr334 amino acid residues at its active sites.[30] The pyrimidine ring of both **NV-1** and **NV-9**, with an *N*-propargyl moiety, is accommodated in the PAS, where one of the phenyl rings containing the methyl group of compound **NV-1** shows π–π stacking interactions with Tyr70. Another phenyl ring of the compound is accommodated in the CAS, where it displays strong π–π stacking interactions with the benzene ring of Phe330 and the 5-membered indole ring of Trp84. NO_2-containing phenyl ring of compound **NV-9** showed π–π and cationic–π interactions with Phe330 and Trp84, respectively, in the CAS region. It confirmed that the test compounds interact with both the CAS and PAS of AChE, thus making them more potent against enzymatic inhibition.

Similarly, both the compounds were docked at hMAO-B (PDB ID-2BYB co-crystallised with pargyline) to determine the binding interactions at the active site of the enzyme. The active site of MAO-B is mainly divided into two cavities, namely, the entrance cavity and the substrate cavity. The side chain of Ile199 separates both the cavities and acts as a gate between them.[31] The pyrimidine ring with the *N*-propargyl moiety of **NV-1** was accommodated in the substrate cavity and was surrounded by Phe99, Phe103, Thr202, and Ser200, while the pyrimidine ring of **NV-9** was situated in the entrance cavity, which was surrounded by Ile198, Ile199, and Tyr326 (Fig. 6). The methyl-containing phenyl ring of the compound **NV-1** was at the entrance cavity, while the other phenyl ring was situated deep within the substrate cavity. Similarly, the trimethoxy phenyl ring of the compound **NV-9** was lying deep within the active substrate cavity, while the nitrophenyl ring showed a cationic–π interaction between the benzene ring of Tyr435 and the nitrogen atom of NO_2 group. Thus, it is evident that the compounds are well accommodated within the cavities and show similar interactions to the standard inhibitor pargyline.

Molecular dynamics simulation studies. Understanding the protein-ligand binding interaction is crucial in the drug design and development process, and molecular dynamics simulation can be used as an effective tool for the identification of potent leads.[32] It is an important tool for understanding the stability

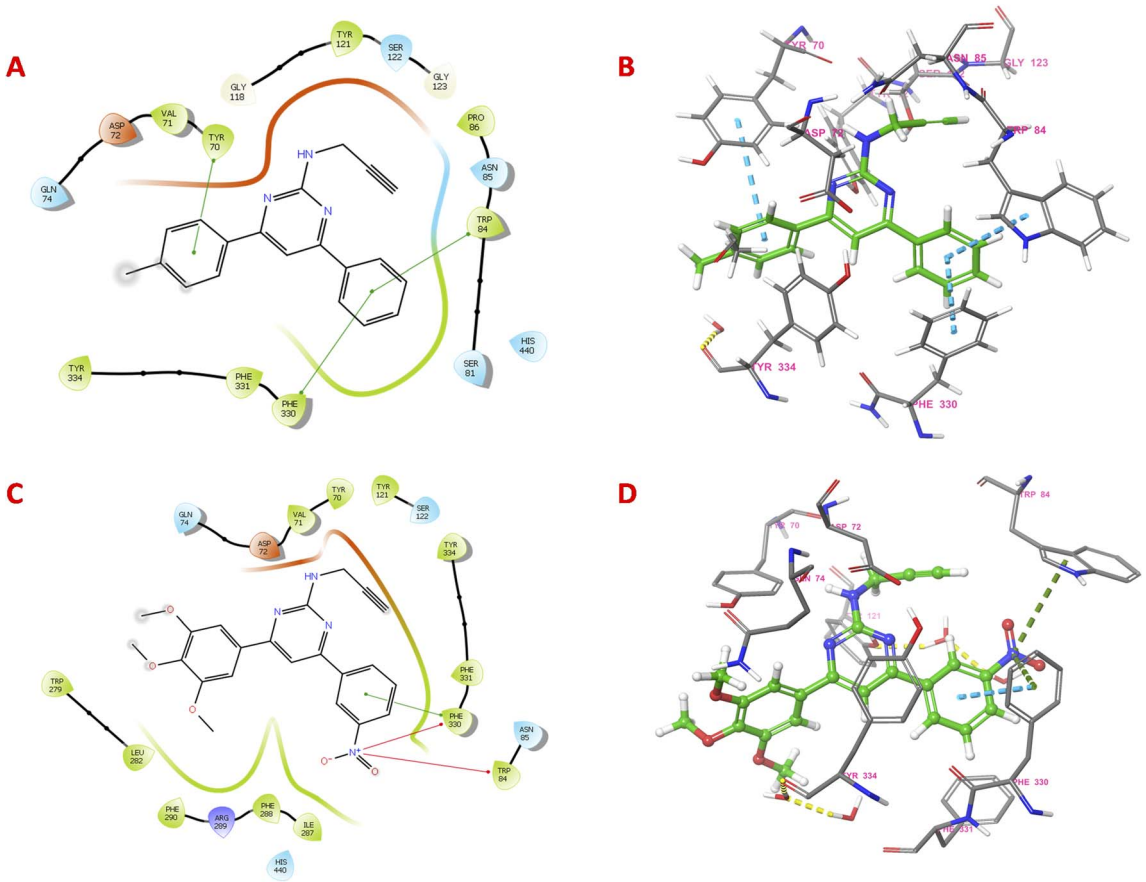

Fig. 5 (A) 2D interactions of **NV-1** with amino acid residues of AChE, (B) 3D binding pattern of **NV-1** with amino acid residues at the active site of AChE, (C) 2D interactions of **NV-9** with amino acid residues of AChE, and (D) 3D binding pattern of **NV-9** with amino acid residues at the active site of AChE.

and conformational changes of ligands within the active cavity of an enzyme. Therefore, the most potent compounds, **NV-1** and **NV-9**, were subjected to MD simulation for 100 ns using GROMACS 2021.3. Fig. 7 depicts the results of the analysis from the MD trajectory of the protein–ligand complex of **NV-9**. Initially, there was a fluctuation in the RMSD plot (Fig. 7A) of the protein between 0.075 and 0.225 nm. Protein RMSD stabilizes between 0.08 and 0.15 nm, and the ligand's RMSD value was found to be extremely stable throughout the simulation ranging from 0.15 to 0.20 nm. The protein and ligand RMSD values were found to be in the acceptable range for both the test compounds, suggesting that the protein and ligand complex was stable throughout the time-period of MD simulation. Additionally, the radius of gyration (Fig. 7B) was calculated to determine the degree of compactness in the structure and to gain insights into the overall dimensions of the protein. The rGy value remained constant throughout the entire trajectory time at 2.32 nm, indicating the high stability of the complex. The stability and flexibility in the protein structure were recorded using RMSF throughout the simulation study to predict the dynamic behavior of the amino acid residues. The analysis of the root mean square fluctuation (RMSF) plot showed that there were no internal fluctuations throughout the simulations, and the interaction RMSF values stayed well within the permissible range of 0.05 to 0.4 nm. The accommodation and stability of the ligand within the catalytic pocket are further supported by the lower RMSF values of the ligand in the range of 0.02–0.18 nm with minimal fluctuation during the simulation (Fig. 7C and D).

Fig. 8 shows the results of the analysis from the MD trajectory of the protein–ligand complex of **NV-1**. Initially, there was a fluctuation in the RMSD plot (Fig. 8A) of the protein between 0.1 and 0.4 nm for 18 ns. After that, it stabilized between 0.4 and 0.42 nm, and the ligand's RMSD value was found to be extremely stable throughout the simulation from 0.075 to 0.12 nm. The protein and ligand RMSD values were within the acceptable range for both the ligands, suggesting that the protein and the ligand were stable throughout the time-period of MD simulation. Additionally, the radius of gyration (Fig. 8B) was calculated to determine the degree of compactness in the structure and to gain insights into the overall dimensions of the protein. This revealed that the complex is highly stable, as the rGy value remains constant throughout the entire trajectory time at 2.33–2.36 nm. The stability and flexibility in the protein structure were recorded using RMSF throughout the simulation study to predict the dynamic behavior of the amino acid residues. The analysis of the root mean square fluctuation (RMSF)

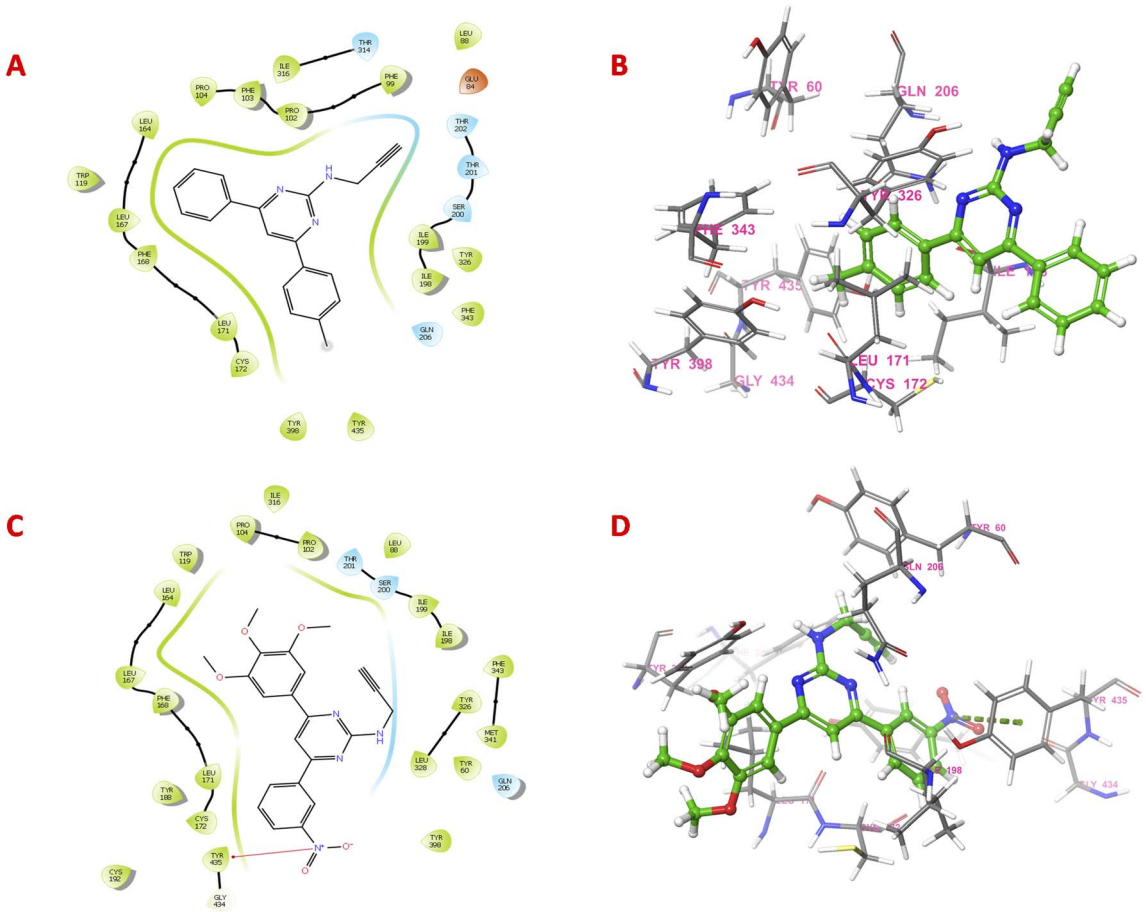

Fig. 6 (A) 2D interactions of **NV-1** with amino acid residues of MAO-B, (B) 3D binding pattern of **NV-1** with amino acid residues at the active site of MAO-B, (C) 2D interactions of **NV-9** with amino acid residues of MAO-B, and (D) 3D binding pattern of **NV-9** with amino acid residues at the active site of MAO-B.

plot showed that there were no internal fluctuations throughout the simulations, and their RMSF values fell well within the permissible range of 0.07 to 0.6 nm. The accommodation and stability of the ligand within the catalytic pocket are further supported by the lower RMSF values of the ligand in the range of 0.02–0.22 nm without much fluctuation (Fig. 8C and D).

Physicochemical properties. For the evaluation of the drug-like characteristics of **NV-1** and **NV-9**, various physiological parameters[33] were calculated using the QikProp application of the Schrodinger software. Both the compounds followed Lipinski's rule of five and showed drug-like properties. The molecular weights of the compounds are below 500. The log *P* values of both the compounds are less than or equal to five. The hydrogen bond donor and hydrogen bond acceptor atoms of compound **NV-1** are less than 5, whereas the hydrogen bond acceptor atoms of compound **NV-9** are 5.75. The QPlogBB values of both the compounds lies within the optimum range of −3.0 to 1.2, and both show 100% human oral absorption.

Lipophilicity evaluation using an octanol-water partition coefficient study. Further, we experimentally, we experimentally evaluated the lipophilicity of the lead compound (**NV-9**) using an octanol/water partition coefficient study (Table S1 and Fig. S1–S3). An HPLC calibration curve was generated to enable accurate and reliable quantification of the compound in both hydrophilic and lipophilic phases. The compound was clearly detected in the octanol phase, whereas no peak was observed in the aqueous phase, indicating a strong preference of the compound for the lipophilic environment. These results support the computational calculation of the log *P* value of 4.42 reported in Table 2. The compound is insoluble in the aqueous phase (precipitated out at the aqueous–organic interface) and hence the log *P* value could not be calculated. Thus, **NV-9** displayed strong binding affinity to AChE, MAO-A, and MAO-B, and in the lipophilicity evaluation studies, this compound was found to be highly lipophilic. A suitable salt formulation of this compound is expected to further improve the BBB permeability and drug-like characteristics.

Structure–activity relationship studies. A series of *N*/*O*-propargyl-substituted diarylpyrimidines were designed and synthesized. A total of 21 molecules were synthesized by varying the substitution pattern at both the aryl rings attached to the pyrimidine scaffold. Various electron-withdrawing and electron-donating substituents were attached to the aryl rings to develop a structure–activity relationship (SAR) profile (Fig. 9). The molecules were evaluated for their inhibitory potential against AChE, MAO-A, and MAO-B. Most of the compounds

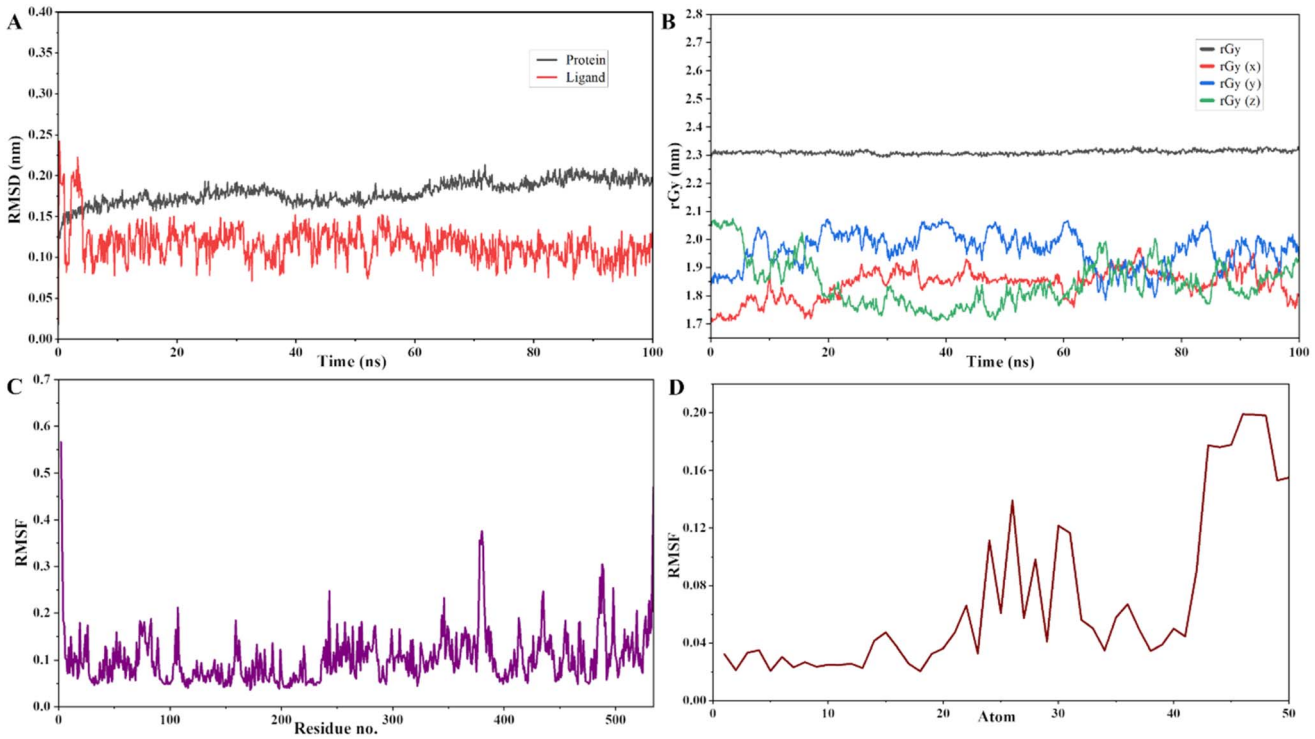

Fig. 7 Molecular dynamics trajectory analysis of the NV9-protein complex. (A) Protein–ligand RMSD; (B) radius of gyration for the complex, (C) RMSF for the protein and (D) RMSF for the ligand.

were active against the AChE enzyme, while selective activity was observed against the MAO-A and MAO-B isoforms. In general, there was no direct correlation between the substitution pattern and MAO-A inhibitory activity; however, *N*-propargylated pyrimidine derivatives were found to be more potent than the *O*-propargylated derivatives against the MAO-B

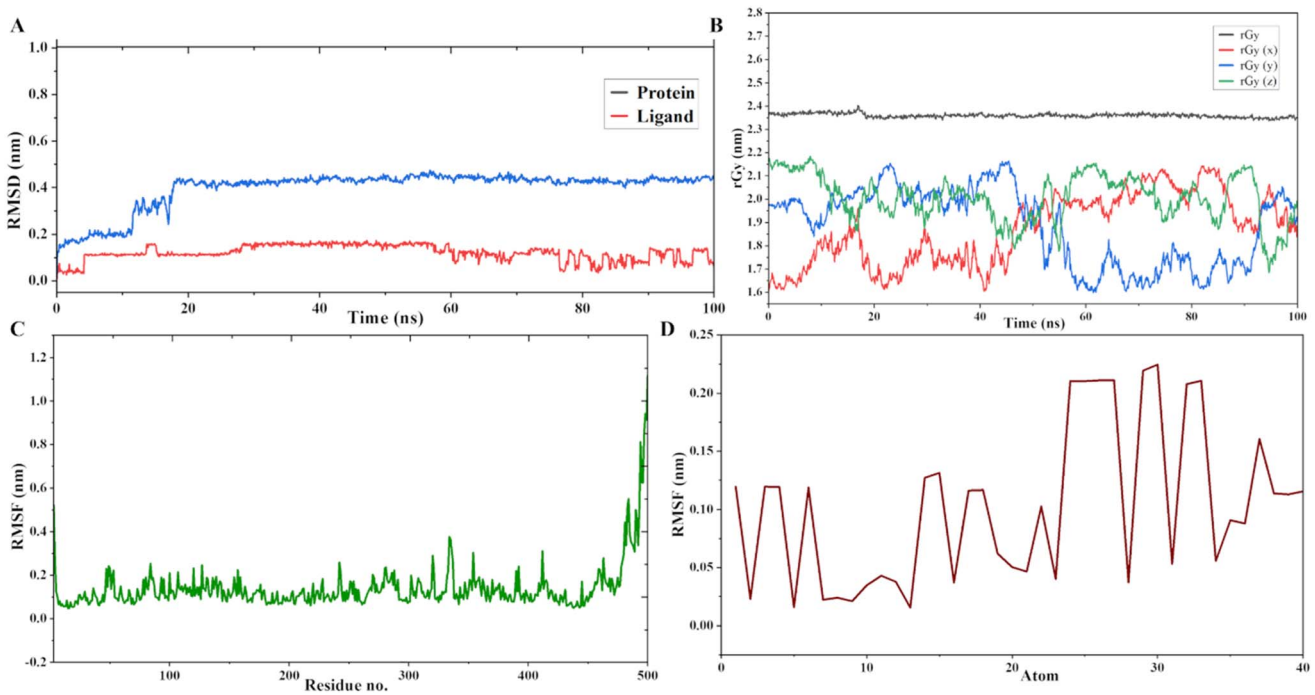

Fig. 8 Molecular dynamics trajectory analysis of the **NV1**-protein complex. (A) Protein–ligand RMSD; (B) radius of gyration of the complex, (C) RMSF for the protein and (D) RMSF for the ligand.

Table 2 Physicochemical properties of the most potent compounds, **NV-1** and **NV-9**[a]

Compound	Mol. wt	Log *P*	HB donor	HB acceptor	% Human oral absorption	QPlogS	QPlogHERG	CNS	QPlogBB (optimum range −3.0 to 1.2)	Predicted BBB permeability
NV-1	299.37	5.05	1.5	2.5	100	−5.91	−6.80	0	−0.085	+ve
NV-9	420.42	4.42	1.5	5.75	100	−6.18	−6.43	−2	−1.417	+ve

[a] +ve = blood–brain barrier permeable and −ve = not permeable for blood–brain barrier.

isoform. On a similar note, no clear correlation was observed between AChE inhibitory activity and the presence of N/O-propargyl substituents on the pyrimidine scaffold. **NV-1** with R_1 as a *para* methyl substituent and R_2 as H was found to be the most potent inhibitor of MAO-A and MAO-B isoforms with IC_{50} values of 0.232 μM and 0.949 μM, respectively. **NV-1** displayed IC_{50} values of 1.30 μM against AChE enzymes. The diaryl rings were substituted with different substituents, such as CH_3, OCH_3, Cl, Br, and NO_2 and no significant improvement in the activity was observed against the target enzymes. **NV-9** with a 3,4,5-tri-OMe substituent on the first aryl ring and 3-NO_2 group on the other aryl ring was found to be the most potent AChE inhibitor with IC_{50} value of 0.88 μM. However, the MAO-A and MAO-B inhibition activity of **NV-9** was found to be reduced, as reported in Table 1. Substitution of either *N*- and *O*-propargylated groups on the pyrimidine ring did not show any direct impact on the AChE inhibitory activity; however, they influenced the MAO-B inhibitory potential of the compounds, whereas the *N*-propargylated derivatives were found to be more potent. Many of the *O*-propargylated compounds (**NV-14**, **NV-15**, and **NV-17** to **NV-21**) were found to be inactive against the MAO-B isoform (IC_{50} > 25 μM). Molecules possessing planar or partially planar architectures can adopt extended conformations that enable simultaneous interaction with both the CAS and the PAS of AChE, while elongated substituents are expected to traverse the flexible gating residues and accommodate within the large substrate cavity of MAO-B. Cationic–π interactions and π–π stacking interactions with

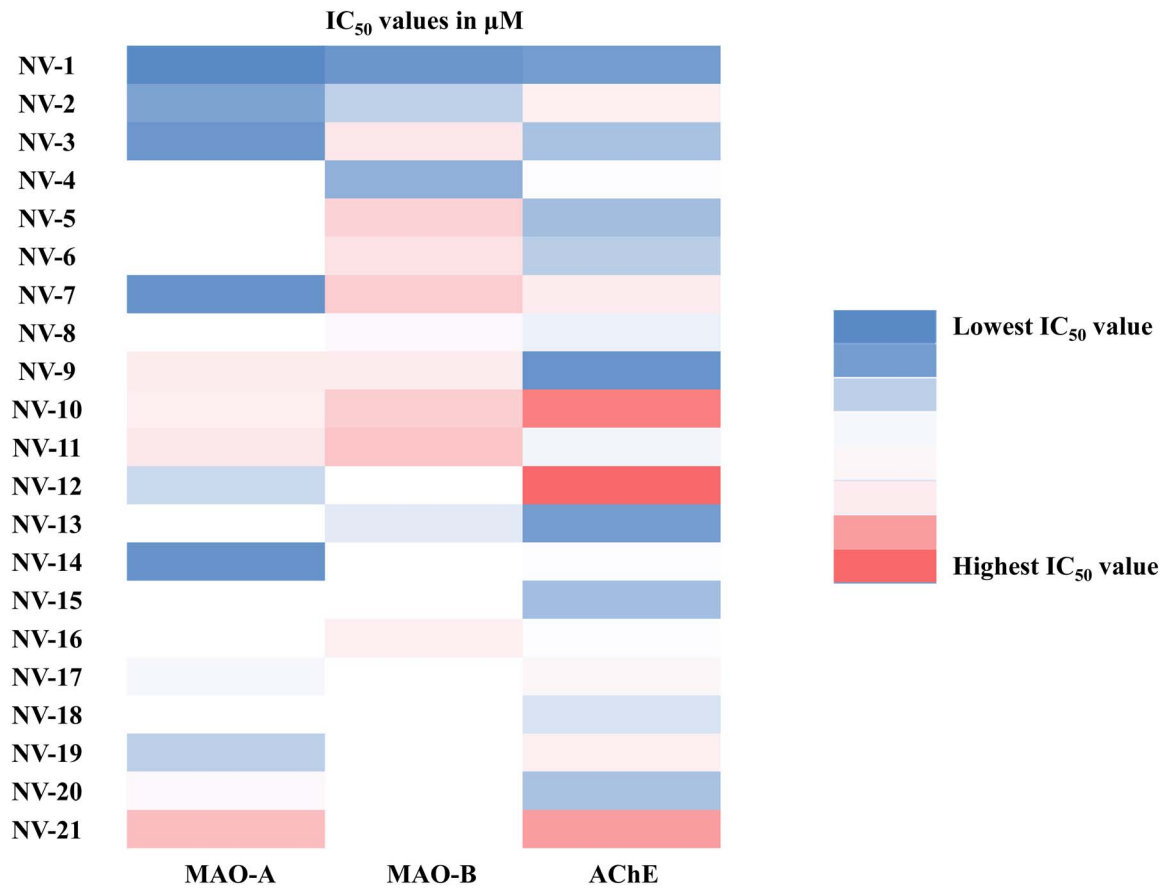

Fig. 9 Heatmap depicting the variation in IC_{50} values of the synthesized derivatives for the structure activity relationship (SAR) against MAO and AChE enzymes. Blue and red colours indicate the most and least potent compounds with the lowest and highest IC_{50} values, respectively. White colour represents inactive compounds at the tested concentrations.

aromatic residues are essential for an enhanced activity profile, and both were observed for the leads in the docking studies. Thus, in this series, **NV-1** and **NV-9** were identified as the most potent derivatives with a balanced activity profile against AChE, MAO-A and MAO-B enzymes.

Conclusion

Alzheimer's disease is associated with multiple pathological hallmarks, and the exact aetiology of the disease is not yet known. It is considered a complex neurodegenerative condition that requires simultaneous inhibition of two or more targets to cure the disease effectively. AChE and MAO are two prime targets involved in the progression of the disease. We synthesized a series of *N*/*O*-propargylated diarylpyrimidines for the simultaneous inhibition of AChE and MAO enzymes. A total of 21 derivatives were synthesized by varying the substitution pattern with either electron-withdrawing or electron-donating groups at both the aryl rings. Amongst the synthesized compounds, **NV-1** displayed the most potent MAO inhibitory activities with IC_{50} values of 0.232 μM and 0.949 μM against MAO-A and MAO-B, respectively. Similarly, **NV-9** was found to be the most potent AChE inhibitor with IC_{50} value of 0.88 μM. It also showed inhibitory activity against MAO-A and MAO-B in the lower micromolar range. In the reversible inhibition studies, both compounds were found to be reversible inhibitors of AChE and MAO enzymes. The compounds are well accommodated within the active sites of enzymes. Although **NV-1** and **NV-9** indicate strong binding affinity to AChE, MAO-A, and MAO-B, based on the *in silico* prediction and lipophilicity evaluation, their BBB permeability could be further improved in future work for these compounds to be considered as drug candidates for AD treatment. In MD simulation studies, compounds **NV-1** and **NV-9** were found to be stable in the active cavities of AChE and MAO enzymes for 100 ns. Thus, the *N*/*O*-propargylated diarylpyrimidines have shown a multipotent activity profile and can be developed as drug candidates for the treatment of AD.

Experimental

Materials and methods

All the chemicals and reagents were purchased from Sigma Aldrich, Avra Synthesis Private Limited, Spectrochem and Qualikems Lifesciences Pvt. Ltd and used as received for the synthesis of the intermediates and target compounds. Glass silica plates coated with GF254 were used for thin-layer chromatography during the monitoring of the reaction. A 1 : 10 and 3 : 10 mixture of ethyl acetate in petroleum ether was used as the solvent for the chromatographic separation and purification of the compounds. For the MAO and AChE inhibition assays, Amplex Red and Ellman's assay kits were purchased from Sigma Aldrich and Molecular Probes, Invitrogen, Life Technologies, India, respectively. SHSY-5Y cell lines were obtained from the National Centre for Cell Science (NCCS), Pune, India. The mass spectra of the synthesized compounds were recorded using electrospray ionisation (ESI) combined with a Q-TOF high resolution mass analyser in a positive ion mode at the Central Instrumentation Laboratory in the Central University of Punjab, Bathinda. ^{1}H and ^{13}C NMR of the purified compounds were recorded in $CDCl_3$ or DMSO at 400 MHz using Bruker's instrument at IIT Ropar and GNDU Amritsar. Tetramethylsilane, TMS ($\delta = 0$), is used as the internal standard with the chemical shifts reported in parts per million (ppm) with respect to TMS. The HRMS of the synthesized compounds was recorded at the Central Instrumentation facility, GNDU Amritsar. A UV-vis spectrophotometer from Shimadzu was used for absorption studies, and a microplate reader from BioTek was used for fluorescence recording. Maestro (Schrodinger) software was utilised for molecular docking and modelling simulation studies.

Chemistry and biological studies

A total of 21 molecules were synthesized by following the synthetic procedure (refer SI) as earlier reported by our research group.[34] All the biological methodology[35–38] and characterization data, including NMR and HRMS, are also available in the SI.

Conflicts of interest

The authors declare no potential conflicts of interest.

Abbreviations

AD	Alzheimer's disease
ACh	Acetylcholine
ADME	Absorption, distribution, metabolism, and excretion
APP	Amyloid precursor protein
Aβ	Amyloid beta
hMAO	Human monoamine oxidase
BuChE	Butyrylcholinesterase
BBB	Blood–brain barrier
CAS	Catalytic active site
ChEs	Cholinesterase
eeAChE	Electric eel acetylcholinesterase
DTNB	5,5′-Dithiobis(2-Nitro Benzoic Acid)
FAD	Flavin adenine dinucleotide
FDA	Food and drug administration
MTDLs	Multi target-directed ligands
nM	Nanomolar
NMDA	*N*-Methyl-D-aspartate
MD	Molecular dynamics
PAS	Peripheral anionic site
IC_{50}	Half maximum inhibition conc
μM	Micromolar

Data availability

The data supporting this article have been included as part of the supplementary information (SI). Supplementary information: a separate supplementary sheet is provided with the synthetic and biological procedures, along with NMR, HRMS

data and graphs of the final compounds. See DOI: https://doi.org/10.1039/d5ra08679e.

Acknowledgements

Vinod Kumar is thankful to the Department of Science and Technology, New Delhi and STARS-IISc (MoE-STARS/STARS-2/2023-0040) for the research grants. NK and Vijay K. are thankful to the University Grants Commission for providing a Senior Research Fellowship. Vinay Kumar and TA are thankful to CSIR for an SRF. KJ is thankful to ICMR (file no. 45/29/2022-/BIO/BMS) for the fellowship grant. Bharti is thankful to DST-WISE for her fellowship. We are thankful to DST for the FIST grant (SR/FST/CS-I/2020/154) and the Central Instrumentation Laboratory of the Central University of Punjab.

References

1 A. D. Korczyn and L. T. Grinberg, Is Alzheimer disease a disease?, *Nat. Rev. Neurol.*, 2024, **20**, 245–251.
2 R. S. Wilson, S. E. Leurgans, P. A. Boyle and D. A. Bennett, Cognitive decline in prodromal Alzheimer disease and mild cognitive impairment, *Arch. Neurol.*, 2011, **68**, 351–356.
3 P. Scheltens, B. De Strooper, M. Kivipelto, H. Holstege, G. Chételat, C. E. Teunissen, J. Cummings and W. M. van der Flier, Alzheimer's disease, *Lancet*, 2021, **397**, 1577–1590.
4 J. Zhang, Y. Zhang, J. Wang, Y. Xia, J. Zhang and L. Chen, Recent advances in Alzheimer's disease: Mechanisms, clinical trials and new drug development strategies, *Signal Transduct. Targeted Ther.*, 2024, **9**, 211.
5 O. Sheppard and M. Coleman, *Alzheimer's Disease: Etiology, Neuropathology and Pathogenesis*, Exon Publications, 2020, pp. 1–21.
6 N. Kumar, V. Kumar, P. Anand, V. Kumar, A. R. Dwivedi and V. Kumar, Advancements in the development of multi-target directed ligands for the treatment of Alzheimer's disease, *Bioorg. Med. Chem.*, 2022, **61**, 116742.
7 I. Ferrer, Hypothesis review: Alzheimer's overture guidelines, *Brain Pathol.*, 2023, **33**, e13122.
8 C. Albertini, A. Salerno, P. de Sena Murteira Pinheiro and M. L. Bolognesi, From combinations to multitarget-directed ligands: A continuum in Alzheimer's disease polypharmacology, *Med. Res. Rev.*, 2021, **41**, 2606–2633.
9 M. Sahu and N. Siddiqui, A review on biological importance of pyrimidines in the new era, *Int. J. Res. Pharm. Sci.*, 2016, **8**, 8–21.
10 S. Singh, M. Dhanawat, S. Gupta, D. Kumar, S. Kakkar, A. Nair, I. Verma and P. Sharma, Naturally inspired pyrimidines analogues for alzheimer's disease, *Curr. Neuropharmacol.*, 2021, **19**, 136–151.
11 T. Mohamed, X. Zhao, L. K. Habib, J. Yang and P. P. Rao, Design, synthesis and structure–activity relationship (SAR) studies of 2, 4-disubstituted pyrimidine derivatives: Dual activity as cholinesterase and Aβ-aggregation inhibitors, *Bioorg. Med. Chem.*, 2011, **19**, 2269–2281.
12 T. Mohamed, J. C. Yeung and P. P. Rao, Development of 2-substituted-N-(naphth-1-ylmethyl) and N-benzhydrylpyrimidin-4-amines as dual cholinesterase and Aβ-aggregation inhibitors: Synthesis and biological evaluation, *Bioorg. Med. Chem. Lett*, 2011, **21**, 5881–5887.
13 S. Ahmad, F. Iftikhar, F. Ullah, A. Sadiq and U. Rashid, Rational design and synthesis of dihydropyrimidine based dual binding site acetylcholinesterase inhibitors, *Bioorg. Chem.*, 2016, **69**, 91–101.
14 S. Manzoor, S. K. Prajapati, S. Majumdar, M. K. Raza, M. T. Gabr, S. Kumar, K. Pal, H. Rashid, S. Kumar and S. Krishnamurthy, Discovery of new phenyl sulfonyl-pyrimidine carboxylate derivatives as the potential multi-target drugs with effective anti-Alzheimer's action: Design, synthesis, crystal structure and in-vitro biological evaluation, *Eur. J. Med. Chem.*, 2021, **215**, 113224.
15 J. Kumar, A. Gill, M. Shaikh, A. Singh, A. Shandilya, E. Jameel, N. Sharma, N. Mrinal, N. Hoda and B. Jayaram, Pyrimidine-Triazolopyrimidine and Pyrimidine-Pyridine Hybrids as Potential Acetylcholinesterase Inhibitors for Alzheimer's Disease, *ChemistrySelect*, 2018, **3**, 736–747.
16 Y.-x. Xu, H. Wang, X.-k. Li, S.-n. Dong, W.-w. Liu, Q. Gong, Y. Tang, J. Zhu, J. Li and H.-y. Zhang, Discovery of novel propargylamine-modified 4-aminoalkyl imidazole substituted pyrimidinylthiourea derivatives as multifunctional agents for the treatment of Alzheimer's disease, *Eur. J. Med. Chem.*, 2018, **143**, 33–47.
17 M. Shahid Nadeem, J. Azam Khan, I. Kazmi and U. Rashid, Design, synthesis, and bioevaluation of indole core containing 2-arylidine derivatives of thiazolopyrimidine as multitarget inhibitors of cholinesterases and monoamine oxidase A/B for the treatment of Alzheimer disease, *ACS Omega*, 2022, **7**, 9369–9379.
18 M. A. Javed, M. S. Jan, A. M. Shbeer, M. Al-Ghorbani, A. Rauf, P. Wilairatana, A. Mannan, A. Sadiq, U. Farooq and U. Rashid, Evaluation of pyrimidine/pyrrolidine-sertraline based hybrids as multitarget anti-Alzheimer agents: In-vitro, in-vivo, and computational studies, *Biomed. Pharmacother.*, 2023, **159**, 114239.
19 S. Pant, R. Kumar K, P. Rana, T. Anthwal, S. M. Ali, M. Gupta, M. Chauhan and S. Nain, Novel substituted pyrimidine derivatives as potential anti-alzheimer's agents: synthesis, biological, and molecular docking studies, *ACS Chem. Neurosci.*, 2024, **15**, 783–797.
20 B. Devi, K. Jangid, V. Kumar, T. Arora, N. Kumar, A. R. Dwivedi, J. Parkash and V. Kumar, Phenylstyrylpyrimidine derivatives as potential multipotent therapeutics for Alzheimer's disease, *RSC Med. Chem.*, 2024, **15**, 2922–2936.
21 V. Kumar, K. Jangid, V. Kumar, N. Kumar, J. Mishra, T. Arora, A. R. Dwivedi, P. Kumar, J. S. Bhatti and J. Parkash, In vitro and in vivo Investigations of 4-Substituted 2-Phenylquinazoline derivatives as multipotent ligands for the treatment of Alzheimer's disease, *Bioorg. Chem.*, 2025, **155**, 108126.
22 B. Kumar, V. Kumar, V. Prashar, S. Saini, A. R. Dwivedi, B. Bajaj, D. Mehta, J. Parkash and V. Kumar, Dipropargyl substituted diphenylpyrimidines as dual inhibitors of

monoamine oxidase and acetylcholinesterase, *Eur. J. Med. Chem.*, 2019, **177**, 221–234.

23 B. Kumar, A. R. Dwivedi, B. Sarkar, S. K. Gupta, S. Krishnamurthy, A. K. Mantha, J. Parkash and V. Kumar, 4, 6-Diphenylpyrimidine derivatives as dual inhibitors of monoamine oxidase and acetylcholinesterase for the treatment of Alzheimer's disease, *ACS Chem. Neurosci.*, 2018, **10**, 252–265.

24 B. Kumar, A. R. Dwivedi, T. Arora, K. Raj, V. Prashar, V. Kumar, S. Singh, J. Prakash and V. Kumar, Design, synthesis, and pharmacological evaluation of N-propargylated diphenylpyrimidines as multitarget directed ligands for the treatment of Alzheimer's disease, *ACS Chem. Neurosci.*, 2022, **13**, 2122–2139.

25 Z. Özdemir, M. A. Alagöz, Ö. F. Bahçecioğlu and S. Gök, Monoamine oxidase-B (MAO-B) inhibitors in the treatment of Alzheimer's and Parkinson's disease, *Curr. Med. Chem.*, 2021, **28**, 6045–6065.

26 J. Reis and C. Binda, The peroxidase-coupled assay to measure MAO enzymatic activity, Monoamine oxidase, *Methods Protoc.*, 2023, 23–34.

27 S. V. Shetab-Boushehri, Ellman's method is still an appropriate method for measurement of cholinesterases activities, *EXCLI J.*, 2018, **17**, 798–799.

28 M. D. Lloyd, Steady-state enzyme kinetics, *Biochemist*, 2021, **43**, 40–45.

29 X.-Y. Meng, H.-X. Zhang, M. Mezei and M. Cui, Molecular docking: a powerful approach for structure-based drug discovery, *Curr. Comput. Aided Drug Des.*, 2011, **7**, 146–157.

30 H. Dvir, I. Silman, M. Harel, T. L. Rosenberry and J. L. Sussman, Acetylcholinesterase: from 3D structure to function, *Chem. Biol. Interact.*, 2010, **187**, 10–22.

31 C. Binda, A. Mattevi and D. E. Edmondson, Structural properties of human monoamine oxidases A and B, *Int. Rev. Neurobiol.*, 2011, **100**, 1–11.

32 M. De Vivo, M. Masetti, G. Bottegoni and A. Cavalli, Role of molecular dynamics and related methods in drug discovery, *J. Med. Chem.*, 2016, **59**, 4035–4061.

33 S. Q. Pantaleão, P. O. Fernandes, J. E. Gonçalves, V. G. Maltarollo and K. M. Honorio, Recent advances in the prediction of pharmacokinetics properties in drug design studies: a review, *ChemMedChem*, 2022, **17**, e202100542.

34 V. Kumar, P. P. Singh, A. R. Dwivedi, N. Kumar, S. C. Sahoo, S. Chakraborty and V. Kumar, Caesium carbonate promoted regioselective O-functionalization of 4, 6-diphenylpyrimidin-2 (1 H)-ones under mild conditions and mechanistic insight, *RSC Adv.*, 2023, **13**, 16899–16906.

35 N. Kumar, K. Jangid, V. Kumar, R. P. Yadav, J. Mishra, S. Upadhayay, V. Kumar, B. Devi, V. Kumar and A. R. Dwivedi, In vitro and in vivo investigations of chromone derivatives as potential multitarget-directed ligands: Cognitive amelioration utilizing a scopolamine-induced zebrafish model, *ACS Chem. Neurosci.*, 2024, **15**, 2565–2585.

36 I. Ferah Okkay, U. Okkay, B. Cicek, A. Yilmaz, F. Yesilyurt, A. S. Mendil and A. Hacimuftuoglu, Neuroprotective effect of bromelain in 6-hydroxydopamine induced in vitro model of Parkinson's disease, *Mol. Biol. Rep.*, 2021, **48**, 7711–7717.

37 S. K. Yusufzai, M. S. Khan, O. Sulaiman, H. Osman and D. N. Lamjin, Molecular docking studies of coumarin hybrids as potential acetylcholinesterase, butyrylcholinesterase, monoamine oxidase A/B and β-amyloid inhibitors for Alzheimer's disease, *Chem. Cent. J.*, 2018, **12**, 1–57.

38 J. Huang, S. Rauscher, G. Nawrocki, T. Ran, M. Feig, B. L. De Groot, H. Grubmüller and A. D. MacKerell Jr, CHARMM36m: an improved force field for folded and intrinsically disordered proteins, *Nat. Methods*, 2017, **14**, 71–73.